View metadata, citation and similar papers at core.ac.uk

brought to you by CORE

provided by Elsevier - Publisher Connector

Coastal Engineering 103 (2015) 52–66

Contents lists available at ScienceDirect

Coastal Engineering

journal homepage: www.elsevier.com/locate/coastaleng

Modelling the morphodynamics of gravel beaches during storms with XBeach-G

R.T. McCall [a,b,*], G. Masselink [a], T.G. Poate [a], J.A. Roelvink [b,c], L.P. Almeida [a]

[a] School of Marine Science and Engineering, Faculty of Science and Engineering, Drake Circus, Plymouth, Devon, PL4 8AA, United Kingdom
[b] Deltares, Rotterdamseweg 185, Delft, 2629 HD, The Netherlands
[c] UNESCO-IHE, Westvest 7, Delft, 2611 AX, The Netherlands

ARTICLE INFO

Article history:
Received 30 December 2014
Received in revised form 7 June 2015
Accepted 18 June 2015
Available online 23 July 2015

Keywords:
Gravel
Shingle
Storm morphology
Overwash
Erosion
Modelling

ABSTRACT

This paper presents an extension of the XBeach-G numerical model with a sediment transport and morphology module, which includes the effect of groundwater ventilation and flow inertia on sediment transport, to simulate the morphodynamic response of pure gravel beaches and barriers to storms. The morphodynamic XBeach-G model is validated by simulating the morphodynamic response of one laboratory and four natural gravel barriers to 10 separate storm events, where the observed morphodynamic response ranged from berm building to barrier rollover. Model results show that XBeach-G is capable of reproducing the type of morphodynamic response of the barrier well in qualitative and quantitative sense (median BSS 0.75), with higher skill for more energetic storm conditions. Inclusion of acceleration forces on coarse gravel beaches is shown to significantly increase model skill and may be essential in modelling these types of beaches. The effect of varying hydraulic conductivity within estimated and published ranges is shown to be of secondary importance. The range of validation cases and lack of site-specific calibration show that XBeach-G can be applied to predict storm impacts on pure gravel beaches and barriers with reasonable to high confidence for a range of hydrodynamic forcing conditions and barrier response types.

© 2015 The Authors. Published by Elsevier B.V. This is an open access article under the CC BY license (http://creativecommons.org/licenses/by/4.0/).

1. Introduction

Gravel beaches and barriers occur on many high-latitude, wave-dominated coasts across the world. Due to their natural ability to dissipate large amounts of wave energy, gravel coasts are widely regarded as a cost-effective and sustainable form of coastal defence (e.g., Aminti et al., 2003; Johnson, 1987). However as demonstrated by the 2013–2014 winter storm season in the UK (Scott et al., in prep), gravel coasts may experience erosion, wave overtopping and even barrier breaching during extreme events, resulting in high societal costs in the form of damages to coastal properties and infrastructure, flooding of the hinterland and loss of lives. In order to effectively assess and maintain coastal safety against storms, coastal managers must be able to predict where and under what conditions coastal flooding will occur, and what measures can be taken to reduce the impact of storms. In a qualitative sense, this knowledge is captured by a widely accepted conceptual model (Fig. 1), in which the morphodynamic response of gravel barriers is related to the ratio between hydrodynamic forcing and the barrier geometry and composition (Bradbury and Powell, 1992; Carter and Orford, 1981; Orford, 1977; Orford and Anthony, 2011; Orford et al., 2003; Powell, 1990). In this model, increasing the relative forcing conditions leads from morphological change of the barrier beach (berm formation, beach erosion), to change at the barrier crest (crest build-up and lowering), or of the entire barrier (barrier rollover). However, in a quantitative sense, our ability to predict the morphodynamic response of gravel coasts to storms is limited (Masselink et al., 2014; Orford and Anthony, 2011).

Currently, coastal managers are largely forced to rely on empirical models to make quantitative predictions of gravel beach storm response and associated flooding risk. These models include empirical models that predict the potential for overtopping and flooding, but do not compute morphological change (e.g., Bradbury, 2000; Matias et al., 2012; Sallenger, 2000), as well as empirical models that describe the cross-shore profile change (e.g., Bagnold, 1940; Bradbury and Powell, 1992; Lorang, 2002; Pilarczyk and Den Boer, 1983; Powell, 1990; Van der Meer, 1992; Van Hijum, 1976; Van Hijum and Pilarczyk, 1982). Although some of these empirical models have been applied with some success in the UK and elsewhere (e.g., Cope, 2005), they are inherently limited in their application by the range of conditions and data from which they are derived (Bradbury et al., 2005, 2011; Obhrai et al., 2008), and the application of these models outside their range of validity has been shown to potentially underestimate the severity of storm impacts (McCall et al., 2013; Van Rijn and

* Corresponding author.
E-mail address: robert.mccall@plymouth.ac.uk (R.T. McCall).

http://dx.doi.org/10.1016/j.coastaleng.2015.06.002
0378-3839/© 2015 The Authors. Published by Elsevier B.V. This is an open access article under the CC BY license (http://creativecommons.org/licenses/by/4.0/).

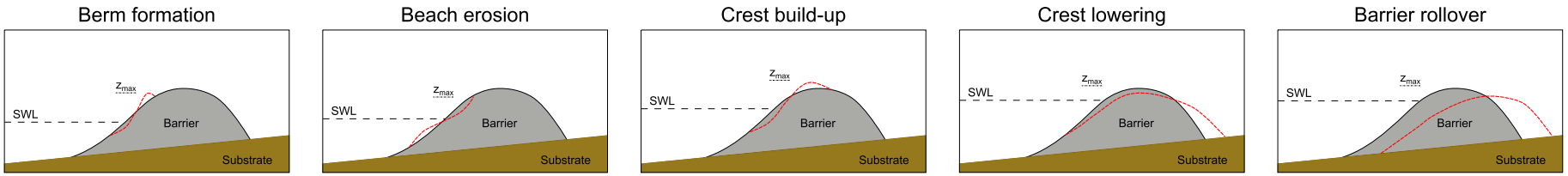

Fig. 1. Conceptual model of the morphological response of a gravel barrier (dashed red line) to varying wave forcing and water levels. From left to right the wave conditions become more energetic and the still water level higher, leading to higher maximum water levels on the barrier (z_{max}). Modified from Orford et al. (2003) and Donnelly (2007).

Sutherland, 2011). Furthermore, since these empirical models have been developed using data from idealised laboratory studies, managed and non-uniform coastlines containing for instance man-made flood defence and beach regulation structures cannot easily be simulated using such models. It is clear that these limitations inhibit the use of such models to make accurate predictions of future storm impacts under changing environmental conditions.

Process-based models offer an improvement over empirical models in that if the underlying physics are well understood and described, these models can essentially be applied in all physical settings governed by those underlying physics. In recent years advancements have been made in the development of process-based models for storm impact on sandy coasts (e.g., Johnson and Grzegorzewski, 2011; Roelvink et al., 2009; Tuan et al., 2006; Van Rijn et al., 2007), but in contrast relatively little advance has been made on those models for gravel coasts. With notable exception of the innovative work of Van Gent (1995, 1996), the development and validation of process-based morphodynamic models for gravel beaches has primarily focussed on low-energy wave conditions and berm formation. While these models in themselves may be considered a step forward relative to empirical models, they may not accurately represent the physics occurring during energetic storm events. Furthermore, due to lack of physical processes such as infiltration (Pedrozo-Acuña et al., 2007; Van Rijn and Sutherland, 2011) and incident band swash dynamics (Jamal et al., 2014; Van Rijn and Sutherland, 2011; Williams et al., 2012b), the ability of these models to accurately predict morphological change depends on the use of artificial, and potentially site and condition-specific, coefficients to adjust important physical processes (e.g., uprush to downwash sediment transport ratio, swash zone velocities, wave run-up levels).

In this paper we attempt to improve current modelling of storm impacts on gravel coasts by presenting a process-based model that is capable of simulating all types of storm impact (Fig. 1) with minimal calibration, building on work by Masselink et al. (2014). The model is validated using data collected during a large-scale physical model experiment (BARDEX; Williams et al., 2012a), as well as storm impact data collected at three gravel beach locations along the UK coast during the 2012–2013 and 2013–2014 storm season as part of the EPSRC-funded NUPSIG[1] project, and at one location on the coast of Brittany (Stéphan et al., 2010). The model presented in this paper is designed and validated only for pure gravel beaches following the classification of Jennings and Shulmeister (2002), although future development of the model would make application on mixed and composite beaches possible.

2. Model description

In this paper we expand the capabilities of an existing open-source, process-based hydrodynamic model for gravel coasts called XBeach-G[2] (McCall et al., 2014) to simulate the morphodynamic response of gravel beaches and barriers to storms. XBeach-G is based on the XBeach model (Roelvink et al., 2009) for sandy coasts, which has previously been modified to (1) solve intra-wave flow and surface elevation variations for waves in intermediate and shallow water depths by means of a one-layer, depth-averaged, non-hydrostatic flow model (Smit et al., 2010), similar to the SWASH model (Smit et al., 2013; Zijlema et al., 2011); and (2) account for upper swash infiltration losses and exfiltration effects on lower swash hydrodynamics on gravel beaches, by means of a non-hydrostatic groundwater model (McCall et al., 2012). The model has been shown to accurately model storm hydrodynamics under a range of hydrodynamic conditions (McCall et al., 2012, 2013, 2014).

[1] New understanding and prediction of storm impacts on gravel beaches (http://www.research.plymouth.ac.uk/coastal-processes/projects/nupsigsite/home.html).

[2] The XBeach-G model discussed in this paper, including the model source code (Fortran95) and a graphical user interface are available for download on the XBeach project website: www.xbeach.org.

In the following section we give a brief description of the surface water flow equations in XBeach-G. Furthermore, we describe the computation of the bed shear stress that is used for the surface flow dynamics and gravel sediment transport, the sediment transport equations, and finally the morphology component of XBeach-G. Although the sediment transport and morphology equations have the potential to be developed in a fully 2DH sense, in this paper we will restrict the description of the equations and application of the models to their 1D equivalent.

2.1. Surface water flow

Depth-averaged flow due to waves and currents is computed using the non-linear shallow water equations, including a non-hydrostatic pressure term and a source term for exchange with the groundwater:

$$\frac{\partial \zeta}{\partial t} + \frac{\partial hu}{\partial x} + S = 0 \tag{1}$$

$$\frac{\partial u}{\partial t} + u\frac{\partial u}{\partial x} - \frac{\partial}{\partial x}\left(\nu_h \frac{\partial u}{\partial x}\right) = -\frac{1}{\rho}\frac{\partial(\rho\bar{q} + \rho g\zeta)}{\partial x} - \frac{\tau_b}{\rho h} \tag{2}$$

where x and t are the horizontal spatial and temporal coordinates respectively, ζ is the free surface elevation above an arbitrary horizontal plane, u is the depth-average cross-shore velocity, h is the total water depth, S is the surface water-groundwater exchange flux (positive for infiltration, negative for exfiltration), ν_h is the horizontal viscosity, ρ is the density of water, $\bar{q}$ is the depth-averaged dynamic pressure normalized by the density, g is the gravitational constant and τ_b is the bed shear stress. We refer to McCall et al. (2014) for a more comprehensive description of the XBeach-G surface water model and its non-hydrostatic extension, and to McCall et al. (2012) for a full description of the XBeach-G groundwater model.

2.2. Bed shear stress

The bed shear stress τ_b is required to compute the surface water momentum balance (Eq. (2)) as well as the Shields parameter for sediment transport (presented later in Eq. (9)). In order to account for the force of the water column on particles in the bed, the bed shear stress is described in terms of a drag and an inertia component (cf. Morison et al., 1950; Puleo et al., 2003). This approach is a modification of that taken by McCall et al. (2014), who only take into account the drag component of the bed shear stress. The modification allows the effect of acceleration on sediment transport to be explicitly taken into account in the bed shear stress, rather than in a modification of the effective Shields parameter (e.g., Nielsen, 2002; Pedrozo-Acuña et al., 2007; Van Gent, 1995):

$$\tau_b = \tau_{bd} + \tau_{bi} \tag{3}$$

where τ_{bd} and τ_{bi} are bed shear stress terms due to drag and inertia, respectively. Note that the inertia component of the bed shear stress does not represent the actual inertia of the particles, but refers to the force on particles in the bed due to pressure gradients, as well as due to the disturbance of the accelerating flow, following potential flow theory (cf. Morison et al., 1950; O'Brien and Morison, 1952). It should be noted that the implementation of this modification has little impact on the hydrodynamic results of McCall et al. (2014), not shown. The bed shear stress component due to drag τ_{bd} is computed using:

$$\tau_{bd} = c_f \rho \frac{u|u|}{h} \tag{4}$$

where c_f is the dimensionless friction factor.

The bed friction factor c_f is computed following the description of Conley and Inman (1994) to account for modified bed shear stress due to ventilated boundary layer effects in areas of infiltration and exfiltration:

$$c_f = c_{f_0}\left(\frac{\Phi}{e^{\Phi}-1}\right) \tag{5}$$

where c_{f0} is the dimensionless bed friction factor without ventilated boundary layer effects, $\Phi = -\frac{1}{2}\frac{b}{c_{f_0}}\frac{S}{|u|}$ is a non-dimensional ventilation parameter and $b = 0.9$ is a constant. Note that the value of the ventilation enhancement and reduction factor $\frac{\Phi}{e^{\Phi}-1}$ is limited to a minimum value of 0.1 and maximum value of 3.0, based on maximum and minimum recorded experimental values (Conley, pers. comm.).

The dimensionless bed friction factor without ventilated boundary layer effects is computed as:

$$c_{f_0} = \frac{g}{\left(18\log\left(\frac{12h}{k}\right)\right)^2} \tag{6}$$

where k is the characteristic roughness height, assumed to be equal to $3D_{90}$, as for flat beds (Van Rijn, 1982). Since the morphodynamic change on gravel beaches is predominantly confined to the swash zone and gravel step, this assumption is considered acceptable to compute storm-induced morphological change. However, it should be noted that the drag component of the bed friction may be underestimated in deeper water, where unresolved sub-grid bed forms may exist.

We compute bed shear due to inertia effects through analogy with the force exerted by water on a sphere in non-stationary flow (cf. Kobayashi and Otta, 1987; O'Brien and Morison, 1952; Van Gent, 1995), which we demonstrate later in this paper to be significant for coarse-grained gravel beaches. In this case, the force on an object due to inertia F_i can be computed from the local flow acceleration:

$$F_i = \rho c_m c_v D^3 \frac{\partial u}{\partial t} \tag{7}$$

where $c_m = 1 + c_a$ is an inertia coefficient, c_a is the added mass coefficient ($c_a = 0.5$ for spheres with zero autonomous acceleration), c_v is the volume shape factor ($c_v = \frac{\pi}{6}$ for spheres) and D is the characteristic grain size. Note that the inertial force is therefore the sum of the Froude–Krylov force ($\rho c_v D^3 \frac{\partial u}{\partial t}$) and the hydrodynamic mass force ($\rho c_a c_v D^3 \frac{\partial u}{\partial t}$). For the purpose of XBeach-G, the shear stress on the bed due to inertia is computed by assuming the characteristic grain size to be the median sediment grain size D_{50} and the number of grains affected by flow acceleration per unit area to scale with $c_n D_{50}^{-2} (c_n \approx \mathcal{O}(1))$ such that:

$$\tau_{bi} = \rho c_m c_v c_n D_{50} \frac{\partial u}{\partial t} \tag{8}$$

Since in most practical cases the individual values of c_m, c_v and c_n cannot be derived from measurement data, these parameters are replaced by one calibration coefficient for inertia $c_i = c_m c_v c_n \approx \mathcal{O}(1)$, which is used to describe the added mass of the grains, as well as the shape of the grains and number of grains on the surface of the bed affected by flow acceleration.

Although Eq. (8) follows the line of reasoning of earlier research, the equation should be considered a proxy for more complex physical processes acting on grains on the bed, including near-bed pressure gradients, boundary layer dynamics, and turbulence. In particular, Eq. (8) ignores the contribution of the advective acceleration term to the total inertia force on particles in the bed, which may be relevant in the swash (cf. Baldock et al., 2005), and does not explicitly account for relative acceleration differences between the surface water and sediment (i.e., dynamic modification of c_a in the hydrodynamic mass force). Despite these simplifications, the application of shear stress on the bed due to inertia following Eq. (8) is demonstrated later in this paper to describe much of the observed morphodynamic response of gravel beaches during storms well, and is of particular importance on coarse-grained gravel beaches.

2.3. Sediment transport

Sediment mobility is defined in XBeach-G using the Shields parameter θ:

$$\theta = \frac{\tau_b}{\rho g \Delta_i D_{50}} \tag{9}$$

where Δ_i is the relative effective weight of the sediment. To account for the effect of through-bed flow on particle weight, the effective weight of the grains is modified by the vertical groundwater pressure gradient according to Turner and Masselink (1998):

$$\Delta_i = \frac{\rho_s - \rho}{\rho} + \alpha\frac{S}{K} = \Delta + \alpha\frac{S}{K} \tag{10}$$

where ρ_s is the density of the sediment, K is the hydraulic conductivity of the bed, and α is an empirical constant relating the surface seepage force to the seepage force in the bed, set to 0.5 in this study following Martin and Aral (1971).

To account for bed slope effects on sediment transport, the effective Shields parameter θ' is modified according to Fredsøe and Deigaard (1992):

$$\theta' = \theta\cos\beta\left(1 \pm \frac{\tan\beta}{\tan\phi}\right) \tag{11}$$

where β is the local angle of the bed, ϕ is the angle of repose of the sediment (approximately 30°–40°), and the right-hand term is less than 1 for up-slope transport, and greater than 1 for down-slope transport.

Sediment transport is computed using the bed load transport equation of Van Rijn (2007), excluding coefficients for silt:

$$q_b = \gamma D_{50} D_*^{-0.3}\sqrt{\frac{\tau_b}{\rho}}\frac{\theta' - \theta_{cr}}{\theta_{cr}}\frac{\tau_b}{|\tau_b|} \tag{12}$$

where q_b is the volumetric bed load transport rate (excluding pore space), γ is a calibration coefficient, set to 0.5 in Van Rijn (2007), $D_* = D_{50}\left(\frac{\Delta g}{\nu^2}\right)^{\frac{1}{3}}$ is the non-dimensional grain size, ν is the kinematic viscosity coefficient of water, and θ_{cr} is the critical Shields parameter for the initiation of transport, computed using the relation of Soulsby and Whitehouse (1997):

$$\theta_{cr} = \frac{0.30}{1 + 1.2D_*} + 0.055\left(1 - e^{-0.020D_*}\right) \tag{13}$$

2.4. Bed level change

Bed level change due to sediment transport is computed from the spatial gradient in the bed load transport (Exner equation):

$$\frac{\partial \xi}{\partial t} + \frac{1}{(1-n)}\frac{\partial q_b}{\partial x} = 0 \tag{14}$$

where ξ is the elevation of the bed above an arbitrary horizontal plane and n is the porosity.

Bed level change due to geotechnical slope collapse is simulated by avalanching material down-slope when the bed slope exceeds the

angle of repose (cf. Roelvink et al., 2009):

$$\begin{aligned} &|\tan\beta| > \phi \quad \textit{avalanching} \\ &|\tan\beta| \le \phi \quad \textit{no avalanching} \end{aligned} \tag{15}$$

3. Case study sites and storm data

The data used in this paper to set-up XBeach-G models and to validate the model results have been collected during a large-scale physical model experiment in the Deltaflume, The Netherlands (BARDEX; Williams et al., 2012a), as well as at three natural gravel beaches along the coast of the UK as part of the NUPSIG-project (Chesil Beach, Loe Bar and Slapton Sands) and one gravel barrier on the Brittany coast (Sillon de Talbert; Stéphan et al., 2010). The location of each site is given in Fig. 2. Although longshore sediment transport may be present at all four natural gravel beaches, the sites selected for this study have been chosen such that the longshore sediment transport gradient during the storm events is expected to have the least effect. A summary of the key hydrodynamic and geometric parameters of the beaches and storms investigated in this paper is given in Table 1.

During the BARDEX physical-model experiment, the hydrodynamics and morphodynamics of a 4-meter high and 50-meter wide barrier composed of medium gravel ($D_{50} = 11\ mm$) were measured under varying hydraulic boundary conditions, ranging from wave run-up to wave overtopping and overwash (see Williams et al., 2012a for details). The morphodynamic response of the gravel barrier to wave action was measured by a mechanical roller and actuator following the bed profile from an overhead carriage before and after each 3–20-minute wave sequence. In this paper we focus on four BARDEX experiment series with significant and distinct morphological change (Table 1 and Fig. 3 for an overview). In BARDEX series BAB3 a berm was generated at the wave run-up extent on an initially plain slope under relatively mild wave conditions. In series BABR, a 3-minute burst of large and long period monochromatic waves was used to remove a berm on the barrier beach in order to generate a smooth and slightly convex beach face. The removal of the berm was accompanied by wave overtopping and accretion on the barrier crest. At the start of series BAE9, overwash of the gravel barrier was triggered by an increase of the offshore water level and wave period. Conditions for overwash increased over the duration of the series through the crest-lowering response of the gravel barrier. Barrier rollover finally occurred during series BAE10, when high wave and water level conditions lead to barrier crest lowering and retreat, and substantial washover deposition on the back barrier (Matias et al., 2012).

Data on the morphodynamic response of three UK gravel beaches to energetic and storm conditions were collected during the winter of 2012–2013 and 2013–2014 as part of the NUPSIG-project (Poate et al., 2015). The three beaches discussed in this paper are Chesil Beach, a coarse ($D_{50} = 40\ mm$) gravel barrier with a crest height approximately 12 meters above ODN (Ordnance Datum Newlyn; approximately equal to 0.2 m below mean sea level – MSL); Loe Bar, a very fine gravel barrier ($D_{50} = 2\ mm$) with a crest height approximately 9 meters above ODN (approximately equal to 0.1 m below MSL); and Slapton Sands, a fine gravel barrier ($D_{50} = 6\ mm$) with a crest height approximately 7 meters above ODN (approximately equal to 0.4 m below MSL). Chesil Beach and Loe Bar have a SW orientation (Fig. 2), and face into the typically SW winter swells, whereas Slapton Sands has an E orientation and is partly sheltered from SW swells.

During CB01 (Table 1 and Fig. 3), Chesil Beach experienced landward migration of the berm under energetic wave conditions combined with spring tides. In CB02, extremely energetic wave conditions lead to beach erosion and approximately 2 meters of scour at the base of a seawall of

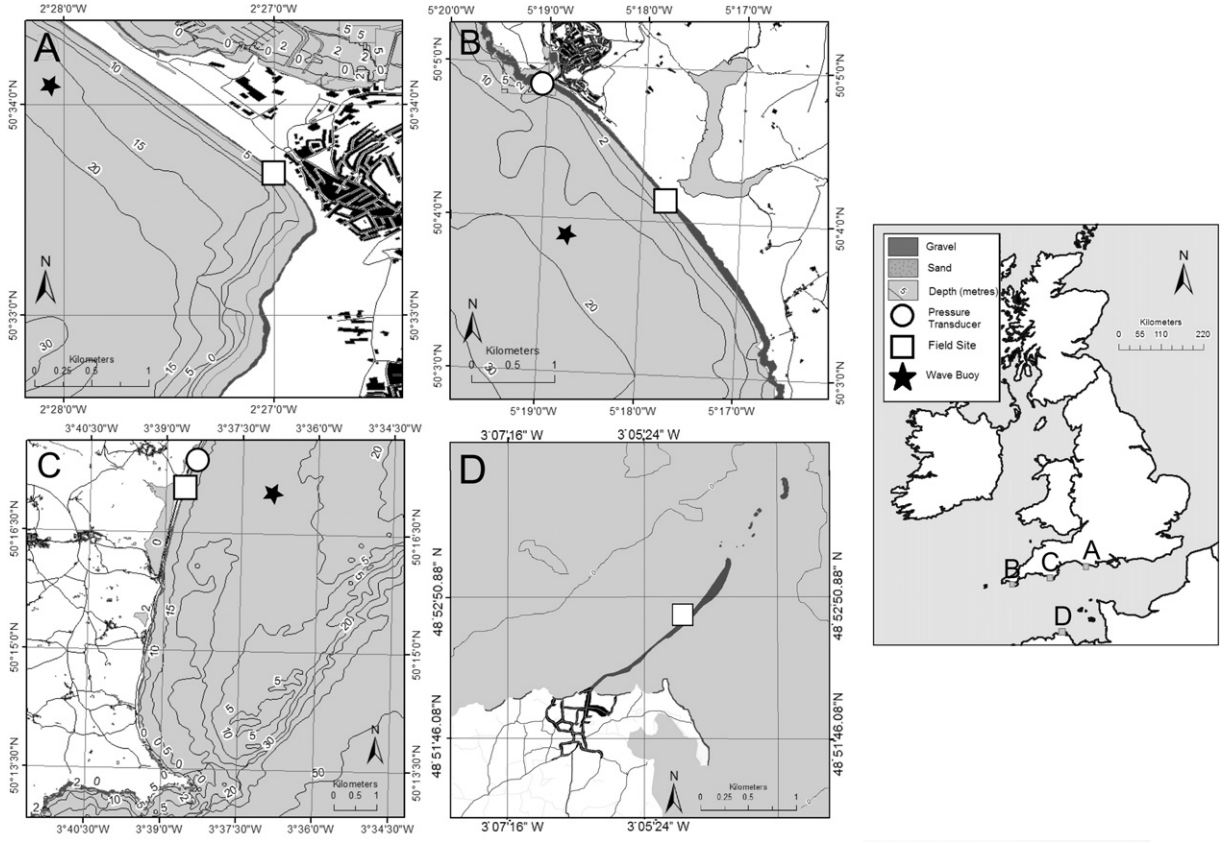

Fig. 2. Location of field data collection sites: (A) Chesil Beach, (B) Loe Bar, (C) Slapton Sands and (D) Sillon de Talbert. Note that the location of the wave buoy at Chesil Beach is beyond the extent of map A and has been depicted at the correct water depth, closer to the field location.

Table 1
Overview of beach characteristics for each of the gravel beach sites, list of storm simulations, maximum hydrodynamic forcing conditions during the storms, and morphological response of the barrier to each of the storm events. In the case of hydraulic conductivity (K), the "high" and "low" estimates are indicated between parentheses. Literature referenced in this table are: a) Williams et al. (2012a), b) Turner and Masselink (2012), c) Heijne and West (1991), d) Hook et al. (1994), e) Carr (1974), f) Poate et al. (2013), g) Poate et al. (2014)), h) Austin et al. (2013), i) Austin and Masselink (2006), j) Austin (2005), k) Stéphan et al. (2010), l) Stéphan et al. (2012), m) Chanson (2006). In the case of BABR § represents monochromatic wave conditions, in the case of CB02 † is relative to the top of the sea wall, and in the case of BAE9, BAE10 and ST01 ‡ is relative to the pre-storm crest level.

Beach characteristics					Storm simulation				Hydrodynamic forcing conditions			Relative forcing and response	
Location	Beach type	D_{50} (mm)	K (mms^{-1})	tan(β)	Simulation	Pre-storm survey	Post-storm survey	Simulation start	Simulation end	Simulated storm duration (h)	H_{m0} (m)	T_p (s)	$[H_{m0}/L_p]_0$	R_c/H_{m0}	Morphodynamic response
BARDEX[a,b]	Coarse gravel barrier	11	155	0.19	BAB3	3 Jul. 2008	3 Jul. 2008	3 Jul. 2008	3 Jul. 2008	1.7	0.8	4.3	0.029	2.0	Berm formation
					BABR	2 Jul. 2008	2 Jul. 2008	2 Jul. 2008	2 Jul. 2008	0.1	1.0§	10.0	0.005	1.0	Crest build-up
					BAE9	28 Jul. 2008	28 Jul. 2008	28 Jul. 2008	28 Jul. 2008	1.2	0.8	8.0	0.007	1.2 ‡	Crest lowering
					BAE10	29 Jul. 2008	29 Jul. 2008	29 Jul. 2008	29 Jul. 2008	1.2	0.8	8.0	0.007	0.5 ‡	Barrier rollover
Chesil Beach[c,d,e]	Coarse gravel beach	40	400 (200–600)	0.20	CB01	14 Dec. 2012	15 Dec. 2012	14 Dec. 2012	15 Dec. 2012	25.0	2.9	8.6	0.027	2.9	Beach erosion and berm formation
					CB02	5 Feb. 2014	6 Feb. 2014	5 Feb. 2014	6 Feb. 2014	21.5	7.6	13.9	0.025	1.0 †	Beach erosion
Loe Bar[f,g,h]	Fine gravel barrier	2	10 (3–30)	0.12	LB01	2 Feb. 2014	18 Feb. 2014	2 Feb. 2014	5 Feb. 2014	64.5	8.0	14.5	0.024	0.6	Crest lowering
Slapton Sands[h,i,j]	Medium gravel barrier	6	75 (19–150)	0.15	SS01	21 Oct. 2013	21 Oct. 2013	21 Oct. 2013	21 Oct. 2013	9.8	2.0	6.9	0.029	2.0	Beach erosion
					SS02	9 Jan. 2014	7 Feb. 2014	4 Feb. 2014	6 Feb. 2014	36.0	4.6	9.5	0.035	0.7	Crest build-up and beach erosion
Sillon de Talbert[k,l,m]	Course gravel barrier	80	400 (200–600)	0.11	ST01	Sep. 2007	Sep. 2008	9 Mar. 2007	12 Mar. 2007	74.0	9.5	16.0	0.024	0.2 ‡	Barrier rollover

Chesil Beach. Eyewitness accounts confirm that other sections of Chesil Beach that were not protected by the seawall experienced wave overtopping and overwash during this event, however these sections are not discussed further in this paper due to lack of morphodynamic data. Offshore wave data for both events were provided by a directional wave buoy maintained by the Channel Coastal Observatory (CCO), located approximately 7 km from the study site in 12–15 m water depth (Fig. 2). Tide data for CB01 were derived from a pressure transducer located at approximately MLWN (ODN - 0.47 m), whereas for CB02 tide data were derived from time series of measured tide and surge at West Bay Harbour tide gauge, approximately 30 km from the study site. During CB01, the morphology of the beach was measured every low tide by RTK-GPS survey, whereas during CB02 the morphology of the beach was continuously measured by a tower-mounted cross-shore laser scanner (see Almeida et al., 2015 for comparable measurements and methodology). Bathymetric data below the elevation of the pre-storm surveys for CB01 and CB02 are derived from hydrographic multibeam survey data collected in 2009 and provided by CCO.

The storm system that caused event CB02, led to overwash at Loe Bar in event LB01, where overwashing waves caused crest lowering of 0.2 m and up to 0.4 m of accretion on the back barrier. Offshore wave data for this event were provided by a directional wave buoy maintained by CCO, located approximately 500 m from the study site in 15–20 m water depth (Fig. 2). Tide and surge data for LB01 were derived from tidal predictions for Loe Bar combined with time series of measured surge at Newlyn tide gauge, approximately 20 km from the study site. Pre-storm topographic data for LB01 were collected two days prior to the storm by means of an RTK-GPS survey. Post-storm topographic data were collected by RTK-GPS survey 13 days after LB01, during which time recovery of the beach took place in the form of a cusp and horn system. Unfortunately, no wave data are available for the period between LB01 and the post-storm survey. However, evaluation of the two nearest CCO wave buoys in operation during this period (Looe Bay and Start Bay) indicate that LB01 was the largest wave event in this period. Eye-witness reports confirm substantial overwash at Loe Bar during LB01 (Earlie, pers. comm.). Bathymetric data below the elevation of the pre-storm survey were collected by singlebeam echosounder survey in March 2012 (cf., Poate et al., 2013).

The morphodynamic response of Slapton Sands to SS01 was characterised by moderate erosion of a berm on the supratidal beach. More substantial morphological change occurred at Slapton Sands during SS02, which was caused by the storm system that led to CB02 and LB01. During SS02, the beach was heavily eroded and the barrier overtopped, leading to temporary closure of the main road on the barrier crest. Offshore wave data for both events were provided by a directional wave buoy maintained by CCO, located approximately 500 m from the study site in 10–15 m water depth (Fig. 2). Tide and surge data for SS01 were collected by a pressure transducer located approximately 1 km from the study site. Tide and surge data for SS02 were derived from tidal predictions for Slapton Sands combined with the magnitude of the measured surge at Devenport and West Bay Harbour tide gauges, approximately 40 km and 80 km from the study site, respectively. Topographic data for SS01 were collected by means of low tide RTK-GPS surveys prior to and following SS01. Pre-storm topographic data for SS02 were collected 27 days prior to the storm by means of an RTK-GPS survey, during which period no wave events above storm threshold were measured by the wave buoy. Post-storm topographic data were collected by RTK-GPS survey 2 days after SS02, during which period washover deposits on the road had been removed to the back barrier. Bathymetric data below the elevation of the pre-storm surveys for SS01 and SS02 are derived from hydrographic singlebeam survey data collected in 2007 and provided by CCO.

Sillon de Talbert is a NW-facing gravel spit on the macro-tidal (maximum tidal range 10.85 m) coast of Brittany, France, fronted by an approximately 1 km-wide intertidal rocky platform. The barrier was heavily overwashed during ST01, when highly energetic wave

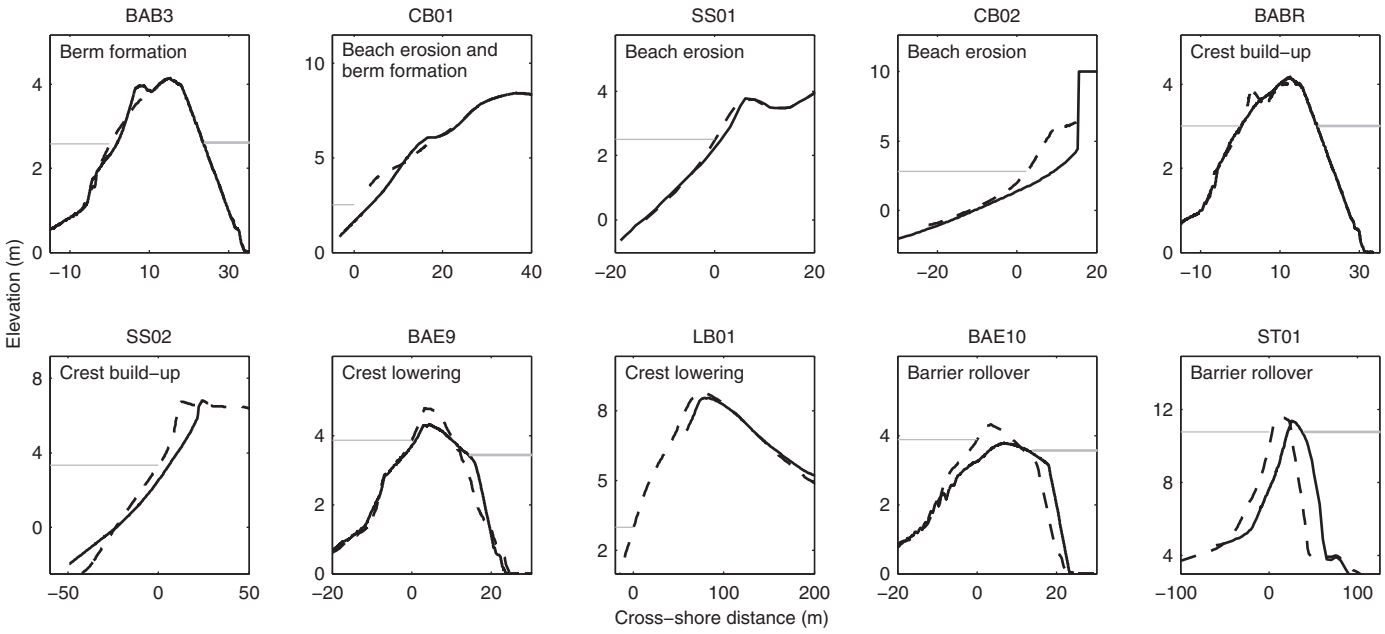

Fig. 3. Overview of the morphological response of the gravel barriers during the 10 storm events discussed in this paper. The panels show the pre-storm cross-shore profile (black dashed), measured post-storm cross-shore profile (black solid) and maximum still water levels (grey lines) for each event. The description in the top left corner of each panel refers to the observed morphological response, see also Fig. 1. Note that the horizontal and vertical scale varies per panel and that detailed plots of each storm event are given in Figs. 4–13.

conditions coincided with spring tide. The storm lead to barrier rollover of approximately 15 m along the central section of the barrier (Stéphan et al., 2010, 2012). Topographic, bathymetric and hydrodynamic forcing conditions for ST01 were provided by l' Université de Bretagne Occidentale (Stéphan and Suanez, pers. comm.). Topographic data of the barrier consist of supratidal and intertidal RTK-GPS measurements of the barrier measured in September 2007 (six months prior to ST01) and September 2008 (six months after ST01). Unpublished cross-shore profile measurements carried out on 19 March 2008 (nine days after the storm) indicate qualitatively that the overall lowering of the crest of the barrier during ST01 was approximately 1 m (Stéphan et al., 2012). These data are supplemented with LiDAR data of the intertidal rocky platform measured in 2002 (Boersma and Hoenderkamp, 2003) and bathymetry data provided by the Service Hydrographique et Océanographique de la Marine. Time series of the storm surge level were derived from surge measured at the Roscoff tide gauge, located approximately 65 km from the study site, alongside tidal predictions at the location of the barrier. Wave conditions offshore of the barrier were extracted from a nested WAVEWATCH III® model (Tolman and Chalikov, 1996), forced by ECMWF wind fields. Model validation results on buoys off Brittany indicate an overall relative root-mean-square error of 12% for wave height with a bias less than 2% (Ardhuin and Accensi, 2011).

A summary of the measured or estimated median grain diameter (D_{50}), hydraulic conductivity (K) and beach slope ($tan(\beta)$) at all five gravel barriers is given in Table 1. The table furthermore lists all storm simulations discussed in this paper, alongside the maximum hydrodynamic forcing conditions (significant wave height at the wave buoy, H_{m0}; peak wave period at the wave buoy, T_p; and the peak deep water wave steepness, $[H_{m0}/L_p]_0$) and a description of the relative forcing and storm morphology (relative freeboard, (R_c/H_{m0}); and the morphodynamic response type) for each of the simulated storms.

4. Model setup

Wave and water level boundary condition time series for the four BARDEX simulations are derived from measured time series of waves imposed at the wave paddle and still water levels measured by pressure transducers on the flume floor (cf. McCall et al., 2014). Wave boundary conditions for the Chesil Beach, Loe Bar, Slapton Sands models are imposed by means of wave spectra time series measured at the nearest wave buoy, and for Sillon de Talbert by means of wave spectrum parameters provided by a large-scale wave model (described in the previous section), both of which XBeach-G uses to internally generate a random time series of incident waves and bound low-frequency second order waves at the model boundary. Tide and surge boundary conditions for these models are derived from measurements (CB01, SS01), or tidal predictions combined with measured surge at locations near the model site (CB02, LB01, SS02, ST01), as described in Section 3.

Where feasible, the model simulations are set up to simulate the entire period of the storm between the pre-storm and post-storm survey (all BARDEX and Chesil Beach simulations, as well as SS01). In these cases, the initial cross-shore profile in the XBeach-G model is set to the cross-shore profile measured at low-tide prior to the simulated storm, or at the start of the simulated wave measurement series. In the case of LB01, the duration of the simulation has been set to the period from the pre-storm measurement to the end of the storm peak, after which no measured wave boundary conditions are available. As discussed in Section 3, this simulation includes the largest storm event of the period between the pre-storm and post-storm measurements, during which the crest lowering and overwash most probably occurred. In the case of SS02, the initial cross-shore profile in the model is set equal to the cross-shore profile measured 27 days before the storm. To reduce computational requirements and to account for the fact that the XBeach-G model is designed to simulate storm events, and does not include processes to model medium to long-term shoreline change (e.g. longshore transport gradients), the duration of the simulation is shortened to 36 hours surrounding the peak of the storm, rather than the duration between surveys (29 days). As discussed in Section 3, no other large wave energy events occurred in the period between the cross-shore profile measurements. In the case of ST01, the initial cross-shore profile is set equal to the cross-shore profile measured 6 months before ST01. Again, for same reasoning as SS02, the duration of the simulation is set to 74 hours surrounding the peak of ST01, rather

than the duration between cross-shore profile measurements (one year). Due to the large period between ST01 and the post-storm profile measurement, the modelled post-storm cross-shore profile cannot be directly compared to the measured change. However, the observed barrier rollover can be attributed to ST01, which was the largest storm event in this period (Stéphan et al., 2010), and the model results can be compared to the measurements in a qualitative sense.

The cross-shore resolution of the models is set to vary gradually in the cross-shore direction, from $\frac{L_m}{25} \approx 2-3\ m$ at the offshore boundary of the model, where L_m is the wave length related to the mean wave period, to 0.3 m near the waterline in order to correctly capture swash processes in the model. In the case of the BARDEX simulations, the resolution has been increased to 0.5 m at the wave generator and 0.1 m at the beach. In the case of CB02 and ST01, the seawall and rocky foreshore, respectively, are included in the cross-shore profile as non-erodible objects.

The hydraulic conductivity and median grain size at BARDEX, Chesil Beach, Loe Bar and Slapton Sands are based on ranges found in literature for these sites (Table 1). Since the reported values of hydraulic conductivity for the natural gravel beaches are relatively uncertain and show considerable spread, all simulations at the natural gravel beaches are computed with three estimates (high, medium and low; Table 1) for the hydraulic conductivity. Due to lack of data for Sillon de Talbert, the median grain size for this barrier is assumed equal to 0.08 m (cf., Chanson, 2006) and the hydraulic conductivity is set equal to that of Chesil Beach, which is the most similar barrier in this study in terms of sediment composition.

The three free model parameters relating to sediment transport are the inertia coefficient (c_i), which acts on sediment transport through the bed shear stress; the angle of repose (ϕ), which controls avalanching and affects sediment transport on sloping beds; and the bed load transport calibration coefficient (γ), which linearly scales transport rates and gradients. Where sufficient data are available, these model parameters can be calibrated at every gravel barrier to provide the most accurate reproduction of measured cross-shore profile change. However, in order to assess the predictive skill of the numerical model we use one value in this paper for the sediment transport parameters ($c_i = 1.0$; $\phi = 35°$; $\gamma = 0.5$) at all four natural gravel sites. In the case of BARDEX, the bed load transport calibration coefficient is modified ($\gamma = 1.0$) in order to capture the apparently highly mobile gravel in the laboratory. Although the reason for the high sediment mobility in the laboratory is uncertain, at this stage it is assumed to be related to the use of angular gravel of fluvial, rather than marine, origin, as well as the 2D nature of the processes, with no longshore smoothing due to variability in swash direction. The remaining two parameters are kept equal to those of the natural gravel sites. All simulations are run using the default values for the hydrodynamic model parameters, as presented by McCall et al. (2014).

5. Model validation

In the following section we discuss the results of the XBeach-G simulations of the storm events presented in Section 3. The results have been grouped according to the morphodynamic response of the gravel barrier: berm formation, beach erosion, crest build-up, crest lowering and barrier rollover (Fig. 1). All model simulations are run using the model parameters described in Section 4. Although higher model accuracy may be achieved by calibration of the free model parameters at each case study site, this is not considered the main objective of this paper.

To assess the skill of the model in simulating morphological change, the cross-shore profile change predicted by the model at the end of the storm event is compared to the measured post-storm cross-shore profile change. As discussed in Section 3, the post-storm profiles for LB01 and ST01 were measured 13 days and 6 months after the respective storm events, during which changes to the beach face (LB01, ST01) and barrier crest (ST01) may have occurred. In these cases the analysis of the model skill is limited to a quantitative (LB01) and qualitative (ST01) analysis of the profile change of the barrier crest and back barrier, and the front of the barrier is not considered. All comparisons at the natural gravel beaches reported in this paper are based on the model simulation corresponding to the "medium" estimate for the hydraulic conductivity, unless stated otherwise.

For all simulations, the absolute profile change prediction error at all points along the profile ($|\epsilon_{\Delta\xi}|$) is computed from the measured and modelled bed level change, as well as an estimate of the measurement error and natural profile variability (ϵ_0), similar to Van Rijn et al. (2003):

$$|\epsilon_{\Delta\xi}| = \max(|\Delta\xi_{modelled} - \Delta\xi_{measured}| - \epsilon_0,\ 0) \tag{16}$$

where $\Delta\xi_{modelled}$ and $\Delta\xi_{measured}$ are the modelled and measured bed level change at each point in the profile, respectively, $\epsilon_0 = \max(\epsilon_i, 3D_{50})$ and ϵ_i is the estimated instrument error (0.030 m for RTK-GPS surveys, 0.015 m for laser scanner data, and 0.005 m for the mechanical roller profiler; cf., Poate et al., 2013; Almeida et al., 2015).

The measured and modelled bed level change and absolute profile change prediction error are subsequently used to compute (1) the root-mean-square error (RMSE; defined in Eq. (17)); (2) the relative bias, normalised by the absolute mean of the observations (Rel. bias; Eq. (18)); (3) the correlation coefficient (ρ; Eq. (19)) and (4) the Brier Skill Score (BSS; Eq. (20)) of the model simulations in a method similar to Roelvink et al. (2009).

$$RMSE = \sqrt{\frac{1}{n}\sum_{i=1}^{n}\left(|\epsilon_{\Delta\xi}|_i\right)^2} \tag{17}$$

$$Rel.\ bias = \frac{\frac{1}{n}\sum_{i=1}^{n}\left(|\epsilon_{\Delta\xi}|_i sgn\left(\Delta\xi_{i,\,modelled} - \Delta\xi_{i,\,measured}\right)\right)}{\frac{1}{n}\sum_{i=1}^{n}\left(|\Delta\xi_{i,\,measured}|\right)} \tag{18}$$

$$\rho = \frac{cov(\Delta\xi_{modelled},\ \Delta\xi_{measured})}{\sigma_{\Delta\xi_{modelled}}\,\sigma_{\Delta\xi_{measured}}} \tag{19}$$

$$BSS = 1 - \frac{\frac{1}{n}\sum_{i=1}^{n}|\epsilon_{\Delta\xi}|_i^2}{\frac{1}{N}\sum_{i=1}^{n}\left(\Delta\xi_{i,\,measured}\right)^2} \tag{20}$$

All statistics are computed using data interpolated to a regularly-spaced grid, and only include points where the measured or modelled bed level changes are greater than ϵ_0.

5.1. Berm formation

Two wave events discussed in Section 3 can be characterised by berm formation: BAB3, where an initially mild beach slope was reworked into steep beach slope with a berm, and CB01, where an existing berm was eroded and a new berm created higher on the beach profile.

The results of BAB3 are shown in Fig. 4. The figure shows that the model can qualitatively reproduce the observed change from a mild beach slope to a steep beach slope with a berm. However, in a quantitative sense, XBeach-G underestimates the volume of the berm, where the volume of the berm accretion is predicted to be 0.4 m^3m^{-1} and the measured berm accretion is 1.4 m^3m^{-1}. The underestimation of the berm volume by XBeach-G is mirrored by an overestimation of sediment deposition below the still water level. Despite these discrepancies, the overall skill of the model prediction is reasonable (Table 2),

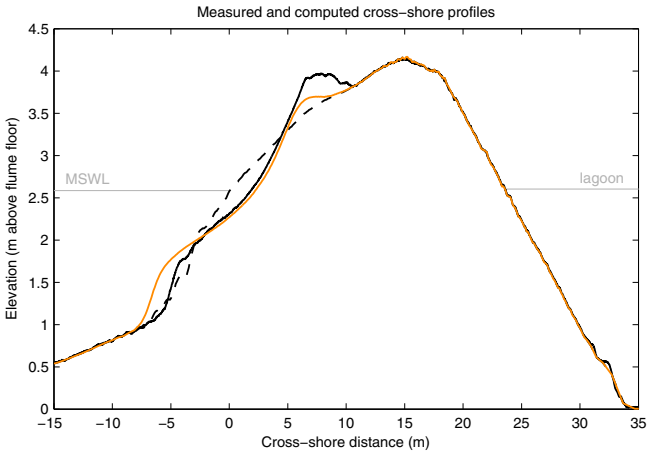

Fig. 4. Initial cross-shore profile (black dashed) and cross-shore profiles measured (black solid) and modelled (orange solid) at the end of wave series BAB3. The maximum still water levels imposed on the front and the back barrier during the simulation are represented by the grey lines.

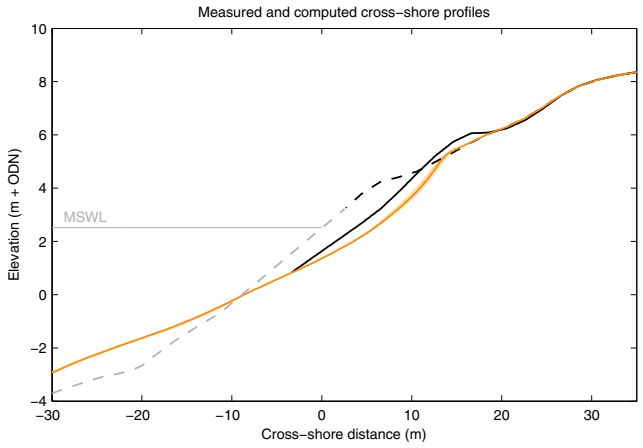

Fig. 5. Pre-storm (black dashed), measured post-storm (black solid) and modelled post-storm (orange solid) cross-shore profiles for CB01. The range in post-storm model profiles due to varying the hydraulic conductivity (Table 1) is shown in light orange shading. The maximum still water level imposed in the simulation is represented by the grey line. The estimated pre-storm profile below the elevation of measurements is represented by a grey dashed line for comparative purposes.

with a BSS of 0.38. Note that BAB3 has low relative bias because the measurements and model results encompass the full mass balance.

The model prediction of cross-shore profile change during CB01 is shown in Fig. 5. The figure shows that the model predicts the erosion of the pre-storm berm, as well as a general steepening of the beach towards a berm-like feature at an elevation of 5 m + ODN. However, in similarity with BAB3, the model greatly under predicts the volume of the post-storm berm above the pre-storm profile (modelled, 0.2 m^3m^{-1}; measured, 2.0 m^3m^{-1}), and the model predicts a more landward position of the post-storm beach. These model discrepancies are reflected in a relatively large model RMSE and relative bias (Table 2), but not by low ρ or BSS values. The latter two represent the fact that despite that the berm is not well represented, the majority of the shape of the cross-shore profile change is captured relatively well by the model.

The results of BAB3 and CB01 show that although XBeach-G is able to reproduce berm formation well in a qualitative sense without site-specific calibration of the model sediment transport parameters, the quantitative skill of the model is not particularly high (median BSS 0.54). Although site-specific calibration of the inertia coefficient (c_i) and angle of repose (ϕ) may change the result of the model prediction at these sites, processes related to wave breaking and gravel step dynamics are likely required to significantly improve model predictions (discussed in Section 6).

Table 2
Root-mean-square error (RMSE), relative bias (Rel. bias), correlation coefficient (ρ) and Brier Skill Score (BSS) of the model cross-shore profile change predictions relative to the measured profile change. Note that ST01 is not included in the statistical analysis and that the comparison of pre- and post-storm profiles for LB01 is limited to the upper part of the beach profile and the barrier crest, see Fig. 11. † refers to the qualification of Van Rijn et al. (2003).

	RMSE	Rel. bias	ρ	BSS (qualifier †)
BAB3	0.16 m	−0.00	0.65	0.38 (fair)
CB01	0.36 m	−0.62	0.98	0.69 (good)
SS01	0.11 m	−0.66	0.96	0.63 (good)
CB02a	0.45 m	−0.71	0.89	0.46 (fair)
CB02b	1.11 m	0.45	0.95	0.77 (good)
CB02c	0.33 m	0.14	1.00	0.98 (excellent)
CB02d	0.17 m	−0.06	0.99	0.99 (excellent)
BABR	0.05 m	−0.00	0.89	0.91 (excellent)
SS02	0.35 m	−0.06	0.92	0.88 (excellent)
BAE9	0.17 m	−0.03	0.83	0.77 (good)
LB01	0.08 m	−0.22	0.99	0.93 (excellent)
BAE10	0.34 m	−0.00	0.82	0.66 (good)

5.2. Beach erosion

Two storm events are characterised primarily by beach erosion: SS01, where an existing berm was partially eroded by energetic waves, and CB02, where substantial beach erosion took place at the base of a sea wall during highly energetic wave conditions.

Fig. 6 shows the modelled and measured cross-shore profiles for SS01. The figure shows approximately 2 m horizontal retreat of the upper beach face above maximum storm still water level due to the partial erosion of the pre-storm berm, which is well reproduced by the XBeach-G model. Between MSL (0.38 m + ODN) and maximum storm still water level, the model slightly overpredicts the magnitude of erosion by approximately 0.2 m. The overall BSS for SS01 is good (0.63; Table 2) and is primarily reduced by the relatively large relative

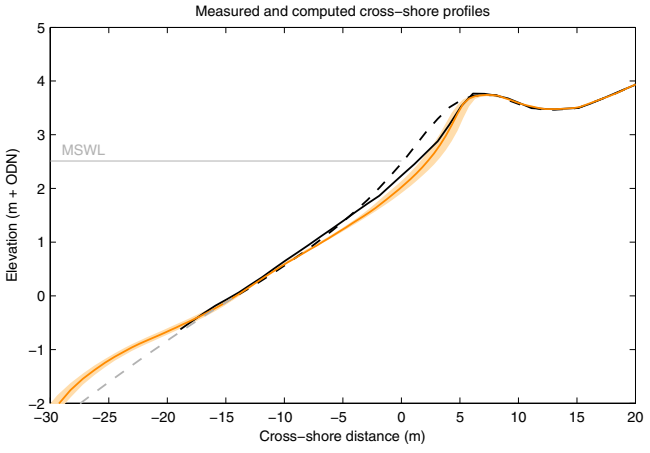

Fig. 6. Pre-storm (black dashed), measured post-storm (black solid) and modelled post-storm (orange solid) cross-shore profiles for SS01. The range in post-storm model profiles due to varying the hydraulic conductivity (Table 1) is shown in light orange shading. The maximum still water level imposed in the simulation is represented by the grey line. The estimated pre-storm profile below the elevation of measurements is represented by a grey dashed line for comparative purposes.

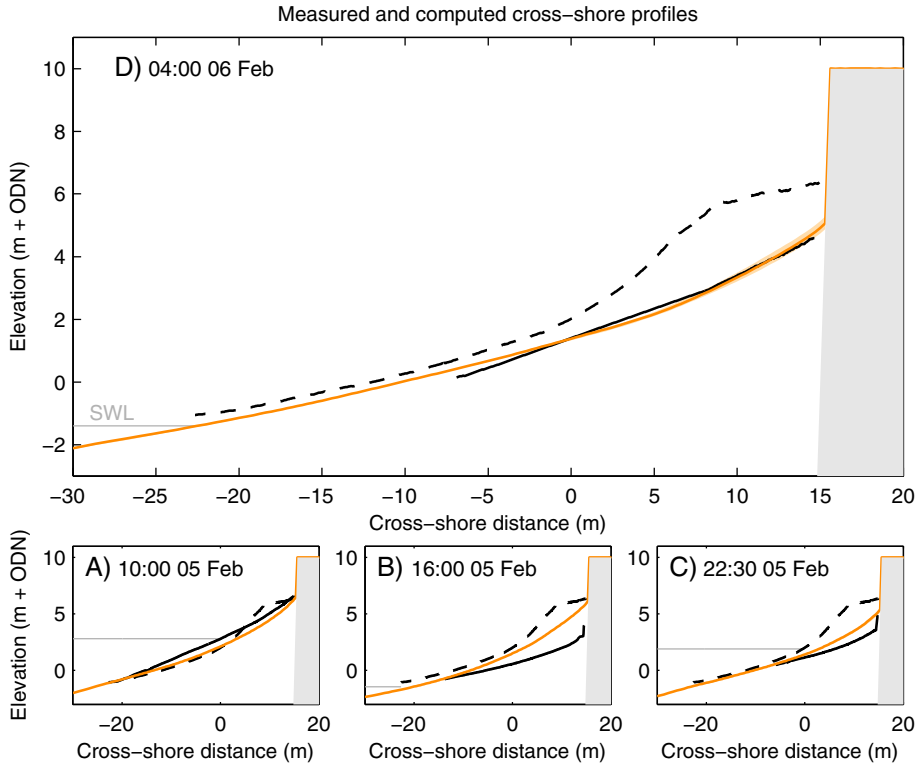

Fig. 7. Pre-storm (black dashed), measured post-storm (black solid) and modelled post-storm (orange solid) cross-shore profiles for CB02. The top panel shows modelled and measured profiles at low tide after CB02 (D). The bottom three panels show from left to right: modelled and measured profiles at the first high tide of CB02 (A), low tide of CB02 (B) and the second high tide of CB02 (C). The range in post-storm model profiles due to varying the hydraulic conductivity (Table 1) is shown in light orange shading. The non-erodible sea wall is shown in grey shading. The tide level for each panel is represented by the grey line.

bias (−66%) caused by the overestimation of beach erosion below maximum still water level.

The morphodynamic impact of CB02 on a beach backed by a sea wall is shown in Fig. 7. The figure shows substantial lowering (~2 *m*) of the post-storm cross-shore profile at the base of the sea wall relative to the pre-storm profile (d; top panel). The figure also shows that the maximum erosion depth at the base of the sea wall was largest at low tide during CB02 (~3 *m*; Fig. 7b, bottom centre panel) when wave conditions were at their most energetic. Fig. 7 and Table 2 show that although the maximum erosion at the base of the seawall is somewhat

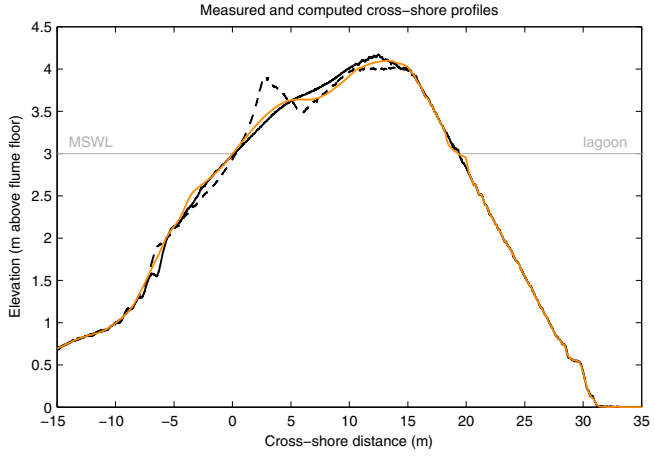

Fig. 8. Initial cross-shore profile (black dashed) and cross-shore profiles measured (black solid) and modelled (orange solid) at the end of wave series BABR. The maximum still water levels imposed on the front and the back barrier during the simulation are represented by the grey lines.

under predicted, XBeach-G generally reproduces the measured cross-shore profile very well (BSS: fair–excellent) and with high ρ values.

5.3. Crest build-up

Two wave events discussed in Section 3 can be principally characterised by crest build-up: BABR (Fig. 8), where an existing berm was reworked by high water levels and energetic waves to the crest, and SS02 (Fig. 9), where energetic waves eroded much of the beach and overtopped the gravel barrier.

Fig. 8 shows up to 0.5 m measured erosion of the berm during BABR between 0 and 5 m cross-shore distance and 0.1–0.2 m deposition on the initially flat barrier crest. The figure shows good agreement between the modelled and measured profile development: the model removes the berm, achieves the correct beach face slope, and deposits sediment on the top of the barrier. This agreement is reflected in the computed and measured erosion (1.0 m^3m^{-1} and 1.1 m^3m^{-1}, respectively) and deposition (0.5 m^3m^{-1} and 0.9 m^3m^{-1}, respectively) above SWL and high BSS (0.91; Table 2).

Fig. 9 shows the modelled and measured cross-shore profiles for SS02. The figure shows substantial beach erosion in the post-storm measurements, leading to a retreat of the crest of 11 m and a thin layer of deposition on top of the barrier. The figure also shows that the results of the XBeach-G model are very similar to the measured cross-shore profile development, expressed in the total eroded volume above maximum still water level (modelled, 31.1 m^3m^{-1}; measured, 31.8 m^3m^{-1}), crest retreat (modelled, 13.9 *m*; measured, 10.7 *m*) and deposition layer thickness on the barrier crest (modelled and measured 0.3 *m*). Although the post-storm beach slope below MSL (0.38 m + ODN) is predicted well by the XBeach model, the beach slope above MSL is less well represented by the model, which is comparable with the results of SS01. The majority of the prediction error on the

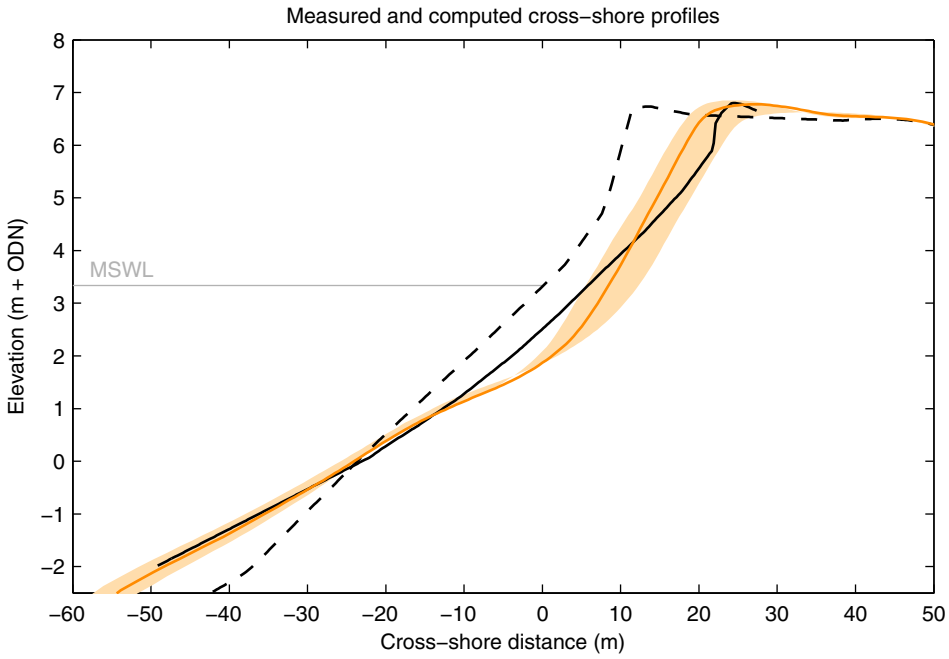

Fig. 9. Pre-storm (black dashed), measured post-storm (black solid) and modelled post-storm (orange solid) cross-shore profiles for SS02. The range in post-storm model profiles due to varying the hydraulic conductivity (Table 1) is shown in light orange shading. The maximum still water level imposed in the simulation is represented by the grey line.

beach slope above MSL however lies within the variation of model predictions due to imposed variations in hydraulic conductivity of the beach. The overall skill of the XBeach-G model for SS02 is high, with a high BSS (0.88; Table 2) and low relative bias (−6%).

5.4. Crest lowering

During BAE9 and LB01 crest lowering and washover occurred under energetic wave conditions in combination with high water levels. During these events the upper part of the barrier beach and crest was eroded, but the crest of the barriers did not move landward significantly.

Fig. 9 shows the modelled and measured cross-shore profiles for BAE9. The measurements show that during BAE9, the crest was lowered by 0.5 m and 4.5 m^3m^{-1} of gravel washed over the crest of the barrier, where washover volume is defined as the volume of sediment accretion landward of the initial barrier crest. The figure shows that in qualitative and quantitative sense, the XBeach-G simulates the observed cross-shore profile change well. The model correctly predicts washover sediment deposition (3.2 m^3m^{-1}) on the back barrier, and lowering of the barrier crest (0.4 m). The model does not quite manage to correctly predict the crest of the barrier, as the model predicts 2.7 m rollback of the crest. Overall, the model skill for BAE9 is high (Table 1), with relatively small RMSE (0.17 m) and high BSS (0.77).

The morphological response of Loe Bar to LB01 is shown in Fig. 11. The figure shows substantial erosion of the the upper beach face and barrier crest, as well as crest lowering and washover deposits on the back barrier (black solid line). Note that the post-storm lower beach face is not shown in the figure due to the recovery of the beach and generation of beach cusps in the period between LB01 and the post-

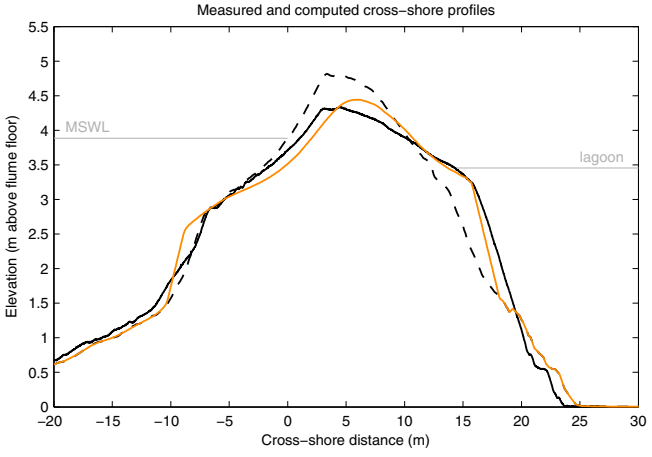

Fig. 10. Initial cross-shore profile (black dashed) and cross-shore profiles measured (black solid) and modelled (orange solid) at the end of wave series BAE9. The maximum still water levels imposed on the front and the back barrier during the simulation are represented by the grey lines.

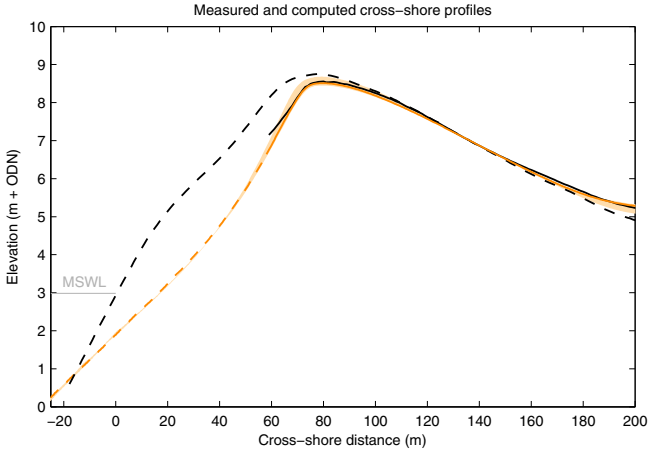

Fig. 11. Pre-storm (black dashed), measured post-storm (black solid) and modelled post-storm (orange solid) cross-shore profiles for LB01. The dashed orange line represents the section of the beach face that may have been reworked in the period between LB01 and the post-storm survey, which is not included in the analysis of the model skill. The range in post-storm model profiles due to varying the hydraulic conductivity (Table 1) is shown in light orange shading. The maximum still water level imposed in the simulation is represented by the grey line.

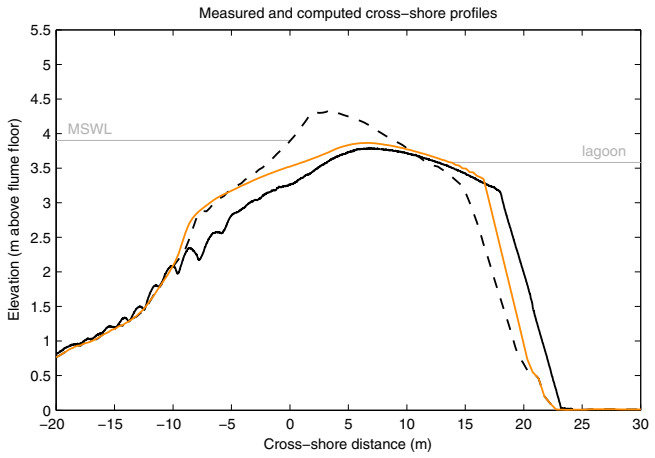

Fig. 12. Initial cross-shore profile (black dashed) and cross-shore profiles measured (black solid) and modelled (orange solid) at the end of wave series BAE10. The maximum still water levels imposed on the front and the back barrier during the simulation are represented by the grey lines.

storm survey, as discussed in Section 3, which is not modelled in XBeach-G. Fig. 11 shows great similarity between modelled and measured post-storm erosion of the barrier crest and deposition on the back barrier. The model correctly predicts a crest lowering of 0.2 m, and predicts crest retreat (modelled, 2.0 m; measured, 1.9 m) and washover volume (modelled, 9.6 m^3m^{-1}; measured, 10.8 m^3m^{-1}) well. The overall model skill for LB01 is high (Table 2), with low RMSE (0.08 m) and high BSS score (0.93).

5.5. Barrier rollover

Barrier rollover occurred during two events discussed in Section 3: BAE10 and ST01, where high water levels and energetic waves lead to crest lowering and substantial crest retreat.

The results of the simulation of BAE10 are shown in Fig. 12. The figure shows a situation with a very low relative freeboard (0.5; Table 1), leading to crest lowering (0.5 m), crest retreat (3.4 m) and substantial washover deposits on the back barrier (8.2 m^3m^{-1}). The results of the simulation show that the XBeach-G model reproduces the observed profile change well in qualitative sense, and reasonably well in quantitative sense. The model predicts lowering and retreat of the barrier crest, as well as washover deposition on the back barrier, although these are all slightly less than found in the measurements (0.5 m, 3.3 m and 4.1 m^3m^{-1}, respectively). The greatest difference between the measurements and the model predictions is the response of the foreshore between −10 m and 0 m cross-shore distance (Fig. 12), where the model under predicts the observed erosion. The lack of erosion in the foreshore leads to an under estimation of washover deposition on the back barrier. Both errors contribute to one of the lowest values of the correlation coefficient (ρ; Table 2) of the simulations discussed in this paper. However, overall model skill remains high for BAE10, with a BSS of 0.66.

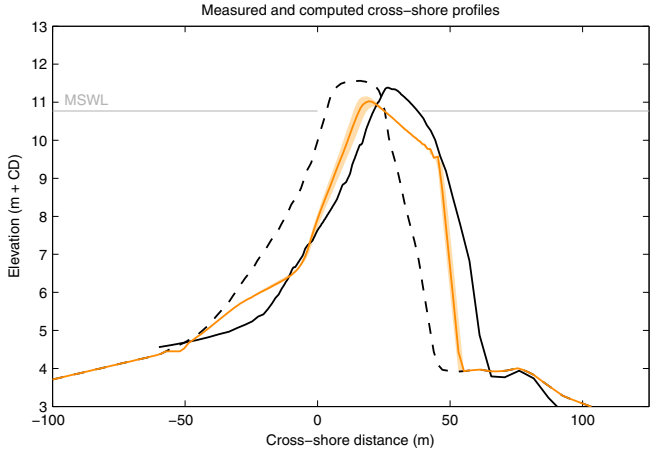

Fig. 13. Pre-storm (black dashed), measured post-storm (black solid) and modelled post-storm (orange solid) cross-shore profiles for ST01. The range in post-storm model profiles due to varying the hydraulic conductivity (Table 1) is shown in light orange shading. The maximum still water level imposed in the simulation is represented by the grey line.

As discussed at the beginning of this section, the period between the pre-storm and post-storm measurement at Sillon de Talbert, as well as the large duration between ST01 and the post-storm measurement, mean that this case cannot be used to validate the XBeach-G model in quantitative sense. However, ST01 was the largest storm event during the period between the pre- and post-storm measurements, and is responsible for the observed barrier rollover (Stéphan et al., 2010). The measured and modelled pre- and post-storm cross-shore profiles of ST01 are shown in Fig. 13. The figure shows a measured crest retreat of 10.7 m, and a washover volume of 130 m^3m^{-1}. The measured crest lowering is just 0.2 m, less than the approximate 1 m lowering measured nine days after ST01 reported by Stéphan et al. (2012), which may be a result of recovery in the six months between ST01 and the post-storm measurements. The results of the model presented in Fig. 13 show good qualitative agreement with the measurements; the model shows crest retreat (3.7 m), crest lowering (0.5 m) and washover deposition (80 m^3m^{-1}) on the back barrier. Since the measurements do not allow for an objective quantitative assessment of the overall model skill, values for the four model skill parameters (Eqs. (17)–(20)) are not presented in Table 2 for ST01.

6. Discussion

The results of the model simulations of 10 storm events discussed in Section 5 show that XBeach-G is able to qualitatively reproduce observed cross-shore profile change for varying hydrodynamic forcing and barrier response types, as well as predict morphodynamic response with high quantitative skill (median BSS 0.75). Interestingly, the results show that the model is more accurate in predicting the response to very energetic storms (beach erosion – barrier rollover; median BSS 0.83) than to less energetic storm conditions (berm formation; median BSS 0.54), although we acknowledge that this may in part be due to the larger observed cross-shore profile changes in the former relative to the reference zero-change prediction (cf., Bosboom et al., 2014). While the model skill for energetic conditions represents a step forward in terms of process-based modelling of gravel beaches, the model may still be improved in certain areas, which are discussed below.

6.1. Berm formation and step development

The results of BAB3 and CB01 show that while XBeach-G is capable of reproducing berm formation in general, the model tends to under predict the volume of the berm. This underestimation is greater or similar to those predicted by other (calibrated) process-based models for varying wave forcing and beach geometries (e.g., Van Gent, 1995; Pedrozo-Acuña et al., 2007; Van Rijn and Sutherland, 2011; Jamal et al., 2014), highlighting a common discrepancy between modelled and naturally-occurring processes. In the case of BAB3, where measured data are available of the submerged profile before and after the wave series, the lack of volume in the post-storm berm is mirrored by an over-estimation of the deposition at, and below, the beach step, leading to the hypothesis that accurate modelling of step dynamics may be required to accurately model berm building. This hypothesis is in line with previous research (refer to Buscombe and Masselink, 2006, for an overview) that

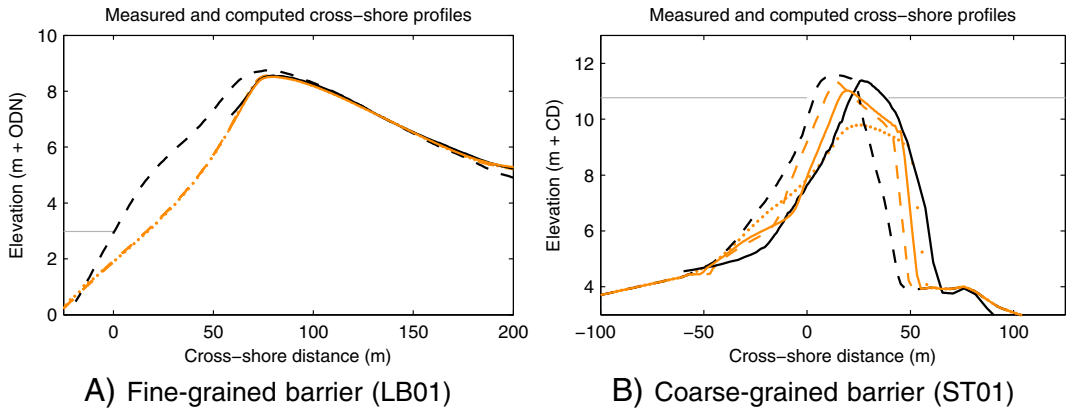

Fig. 14. Sensitivity of modelled cross-shore profile response to the value of the inertia parameter. Pre-storm, measured post-storm and modelled post-storm (default inertia parameter) cross-shore profiles are represented by dashed black, solid black and solid orange lines, respectively. The maximum still water level imposed in the simulation is represented by the grey line. The range in post-storm model profiles due to varying the inertia parameter is shown by dashed orange ($c_i = 2.0$) and dotted orange lines ($c_i = 0.5$).

has highlighted the importance of the step in maintaining steep, reflective beach slopes through preferential onshore sediment transport mechanisms.

Since the hydrodynamics thought to develop and maintain gravel steps is essentially two-dimensional (2DV; e.g., step vortex generation, plunging breakers), representation of these processes in a depth-averaged model presents some difficulties. Important factors not accounted for in the model that all enhance onshore sediment transport across the step region are: (1) bore turbulence; (2) net onshore flow across the seaward face of the step due to the vortex (Larson and Sunamura, 1993); (3) vertical velocity under breaking waves; and potentially (4) breaker pressure pulses (Pedrozo-Acuña et al., 2008). Further steps are envisaged for the development of XBeach-G using a parametrisation of breaker-induced turbulence (cf., Reniers et al., 2013), suspending sediment at wave breaking using the local vertical velocity, and a parametrisation of plunging breaker pressure pulses on the mobilisation of sediment (cf., Pedrozo-Acuña et al., 2010).

6.2. Sensitivity to inertia parameter on coarse-grained beaches

To study the effect of varying the inertia parameter (c_i) on cross-shore profile development in XBeach-G, sensitivity simulations were carried out for a storm event on a fine-grained barrier (LB01) and a storm event on a coarse-grained barrier (ST01). Since the bed shear due to inertia effects scales linearly with the median grain size (Eq. (8)), we expect the sensitivity of the model to the inertia parameter to be greater for ST01 than for LB01. In the sensitivity simulations, the inertia parameter was varied between 0.5–2.0, while all other model parameters were kept constant. The results of these simulations are shown in Fig. 14. The results show that on the fine-grained barrier (left panel), the effect of modifying the inertia parameter is relatively small and does not lead to significantly different cross-shore profile development. However, the response of the coarse-grained barrier (right panel) is strongly affected by the inertia parameter, where a low value of c_i leads to substantially more crest lowering and retreat than measured. This difference is the result of an imbalance between onshore transport (driven by acceleration) and offshore transport (caused by the swash backwash) at the start of the storm, leading to more beach erosion and crest lowering in the case of a low value of c_i, which in turn leads to greater overwash during the peak of the storm.

The result of this sensitivity study highlights the importance of including acceleration forces on coarse-grained gravel beaches in order to model sediment transport magnitudes and directions during storms well (cf., Van Gent, 1995; Pedrozo-Acuña et al., 2007). This importance has previously been found for the threshold of motion of boulders in storms (e.g., Etienne and Paris, 2010) in the equations of Nott (2003) (note however that the equations of Nott do not account for the Froude– Krylov force, resulting in an underestimation of the acceleration forces on boulders under storm waves). Although the current choice of value for the inertia parameter ($c_i = 1$) appears to represent the morphodynamic response of the broad range of gravel barriers discussed in this paper reasonably well, further calibration and validation of the inertia parameter using data collected at coarse-grained beaches would increase confidence in applying the model on coarse gravel and cobble beaches. Such analysis would also highlight the potential for more accurate predictions of morphological change given site-specific calibration of the inertia coefficient.

7. Conclusions

This paper presents an extension of the XBeach-G numerical model (McCall et al., 2014) with a sediment transport and morphology module to simulate the morphodynamic response of pure gravel beaches and barriers to storms. The morphodynamic component of the model computes bed load transport, including groundwater ventilation effects and flow inertia forces, to predict bed level changes. The model is validated by simulating the morphodynamic response of one laboratory and four natural gravel barriers to 10 separate storm events.

Results of the model validation show that the model has considerable skill (median BSS 0.75) in predicting the morphodynamic response of gravel barriers across a wide range of forcing conditions and barrier response types. The results show that the model is most accurate in predicting the response to very energetic storms (beach erosion – barrier rollover; median BSS 0.83). The range of validation cases and lack of site-specific calibration show that XBeach-G can be applied to predict storm impacts on pure gravel beaches and barriers with reasonable to high confidence for a range of hydrodynamic forcing conditions and barrier response types.

Model sensitivity simulations discussed in this paper show that the effect of groundwater infiltration processes, controlled through variation of the hydraulic conductivity within a range of values found in literature, is to modify the magnitude of the cross-shore profile response, rather than to alter the barrier response type. However, it should be noted that in cases where the forcing conditions are at a critical threshold (e.g., beach erosion to crest build-up, and crest build-up to crest lowering) small changes due to groundwater effects may be sufficient to force the beach or barrier system into a different response type. Model sensitivity results furthermore showed the importance of including a term to account for acceleration forces on the bed on course-grained beaches, where simulated onshore transport and morphodynamic response is strongly affected by bed shear stress due to inertia.

Future development of the model should include a focus on validation of the inertia parameter for very coarse gravel and cobbles and investigation of step dynamics that play an important role in controlling onshore sediment transport and swash hydrodynamics under less energetic condition, including in recovery periods. Further co-development of the XBeach and XBeach-G models would make application on mixed and composite beaches possible.

Acknowledgements

The research and data collection in this study were funded by the Engineering and Physical Sciences Research Council (EPSRC; EP/H040056/1 and EP/IO35390/1). In addition, RM and DR would like to acknowledge support given by Deltares (Strategic Research Projects 1202362 and 1209342). Data reported here from the BARDEX experiment were collected in the Delta Flume (Netherlands) as part of the EU-funded BARDEX project (HYDRALAB III Contract no. 022441 (RII3), Barrier Dynamics Experiment). Wave data at the Loe Bar, Chesil Beach and Slapton Sands field sites, as well as bathymetric data at Chesil Beach and Slapton Sands are courtesy of the Channel Coast Observatory. The authors would like to thank the members of the Coastal Processes Research Group at Plymouth University, in particular Pieter Ganderton, Martin Austin and Timothy Scott, for their assistance in the collection of field data and Pieter Smit, Marcel Zijlema and Guus Stelling for their contribution prior to this research in the form of the development of the non-hydrostatic pressure correction term for XBeach. We are particularly indebted to Serge Suanez and Pierre Stephan for the provision of data for the modelling of Sillon de Talbert. Finally, we would like to thank two anonymous reviewers for their improvements to this paper.

References

Almeida, L., Masselink, G., Russell, P., Davidson, M., 2015. Observations of gravel beach dynamics during high energy wave conditions using a laser scanner. Geomorphology 228 (0), 15–27 (http://www.sciencedirect.com/science/article/pii/S0169555X14004279).

Aminti, P., Cipriani, L.E., Pranzini, E., 2003. Back to the beach: converting seawalls into gravel beaches. In: Goudas, C., Katsiaris, G., May, V., Karambas, T. (Eds.), Soft shore protection. Vol. 7 of Coastal systems and continental margins. Springer, Netherlands, pp. 261–274.

Ardhuin, F., Accensi, M., 2011. Etats de mer et agitation sur le fond dans la sous-région marine manche, mer du nord dcsmm/ei/mmn. ref. dcssm/ei/ee/mmn/1.1.7/2011. Tech. rep. Ministère de l'Ecologie du Développement Durable des Transports et du Logement.

Austin, M., 2005. Swash, groundwater and sediment transport processes on a gravel beach Ph.D. thesis Loughborough University.

Austin, M., Masselink, G., 2006. Swash-groundwater interaction on a steep gravel beach. Cont. Shelf Res. 26 (20), 2503–2519 (http://www.sciencedirect.com/science/article/pii/S0278434306002809).

Austin, M.J., Masselink, G., McCall, R.T., Poate, T.G., 2013. Groundwater dynamics in coastal gravel barriers backed by freshwater lagoons and the potential for saline intrusion: Two cases from the UK. J. Mar. Syst. 123–124 (0), 19–32 (http://www.sciencedirect.com/science/article/pii/S0924796313000870).

Bagnold, R., 1940. Beach formation by waves; some model-experiments in a wave tank. J. ICE 15, 27–52.

Baldock, T.E., Barnes, M., Hughes, M.G., 2005. Field observations of instantaneous cross-shore free surface profiles and flow depths in the swash zone.

Boersma, S.M., Hoenderkamp, K., 2003. Tregor, final report. Tech. rep. IFREMER.

Bosboom, J., Reniers, A., Luijendijk, A., 2014. On the perception of morphodynamic model skill. Coast. Eng. 94, 112–125 (http://www.sciencedirect.com/science/article/pii/S0378383914001604).

Bradbury, A.P., 2000. Predicting breaching of shingle barrier beaches – recent advances to aid beach management. Papers and Proceedings 35th MAFF (DEFRA) Conference of River and Coastal Engineers (pp. 05.3.1 – 05.3.13).

Bradbury, A., Powell, K.A., 1992. The short-term profile response of shingle spits to storm wave action. Proc. 23rd International Conference on Coastal Engineering, pp. 2694–2707.

Bradbury, A., Cope, S., Prouty, D., 2005. Predicting the response of shingle barrier beaches under extreme wave and water level conditions in Southern England. Proc. 5th International Coastal Dynamics Conference. American Society of Civil Engineers, Reston, Virginia.

Bradbury, A., Stratton, M., Mason, T., 2011. Impacts of wave climate with bi-modal wave period on the profile response of gravel beaches. Proceedings of Coastal Sediments. World Scientific vol. 3, pp. 2004–2018.

Buscombe, D., Masselink, G., 2006. Concepts in gravel beach dynamics. Earth Sci. Rev. 79, 33–52 (http://www.sciencedirect.com/science/article/pii/S0012825206000791).

Carr, A., 1974. Differential movement of coarse sediment particles. Proceedings of 14th Conference on Coastal Engineering, Copenhagen, Denmark, pp. 851–870 (https://icce-ojs-tamu.tdl.org/icce/index.php/icce/article/view/2944).

Carter, R.W.G., Orford, J.D., 1981. Overwash processes along a gravel beach in South-East Ireland. Earth Surf. Process. Landf. 6 (5), 413–426. http://dx.doi.org/10.1002/esp.3290060503.

Chanson, H., 2006. The Sillon de Talbert, Cotes d'Armor, North Brittany, France. Shore Beach 74 (3), 26–27.

Conley, D.C., Inman, D.L., 1994. Ventilated oscillatory boundary layers. J. Fluid Mech. 273, 261–284.

Cope, S., 2005. Predicting overwashing and breaching of coarse-clastic barrier beaches and spits - application to Medmerry, West Sussex, Southern England. Proc. 5th International Coastal Dynamics Conference. American Society of Civil Engineers, Reston, Virginia, USA.

Donnelly, C., 2007. Morphologic change by overwash: Establishing and evaluating predictors. International Coastal Symposium. Vol. ICS2007 (Proceedings). Journal of Coastal Research. Gold Coast, Australia, pp. 520–526.

Etienne, S., Paris, R., 2010. Boulder accumulations related to storms on the south coast of the Reykjanes Peninsula (Iceland). Geomorphology. rock Coast Geomorphology 114, pp. 55–70 (http://www.sciencedirect.com/science/article/pii/S0169555X09000749).

Fredsøe, J., Deigaard, R., 1992. Mechanics of coastal sediment transport. Advanced series on ocean engineering vol.3. World Scientific, Singapore.

Heijne, I., West, G., 1991. Chesil sea defence scheme. paper 2: design of interceptor drain. Proc. Inst. Civ. Eng. 90, 799–817.

Hook, B.J., Kemble, J.R., Heijne, I.S., Wes, G.M., 1994. Chesil sea defence scheme: Concept, design and construction, and design of interceptor drain. discussion of papers 9611 & 9657. Proc. ICE Water Marit. Energy 106 (4), 385–391.

Jamal, M.H., Simmonds, D., Magar, V., 2014. Modelling gravel beach dynamics with XBeach. Coast. Eng. 89, 20–29.

Jennings, R., Shulmeister, J., 2002. A field based classification scheme for gravel beaches. Mar. Geol. 186, 211–228 (http://www.sciencedirect.com/science/article/pii/S0025322702003146).

Johnson, C.N., 1987. Rubble beaches versus rubble revetments. Proceedings ASCE Conference on Coastal Sediments 1987. American Society of Civil Engineers, Reston, Virginia, USA, pp. 1216–1231.

Johnson, B., Grzegorzewski, A., 2011. Modeling nearshore morphologic evolution of Ship Island during Hurricane Katrina. Proceedings of coastal sediments. World scientific, pp. 1797–1810.

Kobayashi, N., Otta, A.K., 1987. Hydraulic stability analysis of armor units. J. Waterw. Port Coast. Ocean Eng. 113 (2), 171–186.

Larson, M., Sunamura, T., 1993. Laboratory experiment on flow characteristics at a beach step. J. Sediment. Res. 63 (3), 495–500.

Lorang, M.S., 2002. Predicting the crest height of a gravel beach. Geomorphology. 29th Binghamton Geomorphology Symposium: Coastal Geomorphology 48, pp. 87–101 (http://www.sciencedirect.com/science/article/pii/S0169555X02001769).

Martin, C., Aral, M., 1971. Seepage force on interfacial bed particles. J. Hydraul. Div. 7, 1081–1100.

Masselink, G., McCall, R., Poate, T., van Geer, P., 2014. Modelling storm response on gravel beaches using XBeach-G. Proc. ICE Marit. Eng. 167 (18), 173–191 (http://www.icevirtuallibrary.com/content/article/10.1680/maen.14.00020).

Matias, A., Williams, J., Masselink, G., Ferreira, O., 2012. Overwash threshold for gravel barriers. Coastal engineering. BARDEX: a large-scale laboratory study of gravel barrier dynamics 63, pp. 48–61 (http://www.sciencedirect.com/science/article/pii/S0378383911001980).

McCall, R., Masselink, G., Roelvink, J., Russell, P., Davidson, M., Poate, T., 2012. Modeling overwash and infiltration on gravel barriers. Proceedings of the 33rd International Conference on Coastal Engineering.

McCall, R., Masselink, G., Poate, T., Bradbury, A., Russell, P., Davidson, M., 2013. Predicting overwash on gravel barriers. Journal of Coastal Research Special Issue No. 65 Proceedings 12th International Coastal Symposium, pp. 1473–1478.

McCall, R., Masselink, G., Poate, T., Roelvink, J., Almeida, L., Davidson, M., Russell, P., 2014. Modelling storm hydrodynamics on gravel beaches with XBeach-G. Coast. Eng. 91, 231–250 (http://www.sciencedirect.com/science/article/pii/S0378383914001288).

Morison, J., O'Brien, M., Johnson, R., Schaaf, S., 1950. The force exerted by surface waves on piles. Petroleum Transactions, American Institute of Mining and Metallurgical Engineers. 189 pp. 149–154.

Nielsen, P., 2002. Shear stress and sediment transport calculations for swash zone modelling. Coast. Eng. 45, 53–60.

Nott, J., 2003. Waves, coastal boulder deposits and the importance of the pre-transport setting. Earth Planet. Sci. Lett. 210, 269–276 (http://www.sciencedirect.com/science/article/pii/S0012821X03001043).

O'Brien, M., Morison, J., 1952. The forces exerted by waves on objects. Trans. Am. Geophys. Union 33 (1), 32–38.

Obhrai, C., Powell, K., Bradbury, A., 2008. A laboratory study of overtopping and breaching of shingle barrier beaches. Proceedings of 31st International Conference on Coastal Engineering. World Scientific, Singapore.

Orford, J.D., 1977. A proposed mechanism for storm beach sedimentation. Earth Surf. Process. 2 (4), 381–400. http://dx.doi.org/10.1002/esp.3290020409.

Orford, J.D., Anthony, E.J., 2011. Extreme events and the morphodynamics of gravel-dominated coastal barriers: Strengthening uncertain ground. Mar. Geol. 290, 41–45 (http://www.sciencedirect.com/science/article/pii/S0025322711002325).

Orford, J., Jennings, R., Pethick, J., 2003. Extreme storm effect on gravel-dominated barriers. Proceedings of the International Conference on Coastal Sediments.

Pedrozo-Acuña, A., Simmonds, D.J., Chadwick, A.J., Silva, R., 2007. A numerical-empirical approach for evaluating morphodynamic processes on gravel and mixed sand-gravel beaches. Mar. Geol. 241, 1–18 (http://www.sciencedirect.com/science/article/pii/S0025322707000606).

Pedrozo-Acuña, A., Simmonds, D.J., Reeve, D.E., 2008. Wave-impact characteristics of plunging breakers acting on gravel beaches. Mar. Geol. 253, 26–35 (http://www.sciencedirect.com/science/article/pii/S0025322708001473).
Pedrozo-Acuña, A., Torres-Freyermuth, A., Zou, Q., Hsu, T.-J., Reeve, D.E., 2010. Diagnostic investigation of impulsive pressures induced by plunging breakers impinging on gravel beaches. Coast. Eng. 57 (3), 252–266 (http://www.sciencedirect.com/science/article/pii/S0378383909001495).
Pilarczyk, K., Den Boer, K., 1983. Stability and profile development of coarse material and their application in coastal engineering. Tech. rep.Delft Hydraulics
Poate, T., Masselink, G., Davidson, M., McCall, R., Russell, P., Turner, I., 2013. High frequency in-situ field measurements of morphological response on a fine gravel beach during energetic wave conditions. Mar. Geol. 342, 1–13 (http://www.sciencedirect.com/science/article/pii/S0025322713000959).
Poate, T., Masselink, G., McCall, R., Russell, P., Davidson, M., 2014. Storm-driven cusp behaviour on a high energy gravel beach. Journal of Coastal Research Special Issue 70, Proceedings 13th International Coastal Symposium, pp. 645–650 (Durban, South Africa).
Poate, T., Masselink, G., McCall, R., Russell, P., Davidson, M., 2015. UK storms 2014: Gravel beach response. Proceedings of Coastal Sediments 2015, San Diego.
Powell, K.A., 1990. Predicting short term profile response for shingle beaches. Tech. rep., HR Wallingford SR report 219.
Puleo, J., Holland, K., Plant, N., Slinn, D., Hanes, D., 2003. Fluid acceleration effects on suspended sediment transport in the swash zone. J. Geophys. Res. Oceans 108 (C11) (1978–2012).
Reniers, A.J.H.M., Gallagher, E.L., MacMahan, J.H., Brown, J.A., van Rooijen, A.A., van Thiel de Vries, J.S.M., van Prooijen, B.C., 2013. Observations and modeling of steep-beach grain-size variability. J. Geophys. Res. Oceans 118 (2), 577–591. http://dx.doi.org/10.1029/2012JC008073.
Roelvink, J.A., Reniers, A., van Dongeren, A.R., van Thiel de Vries, J.S.M., McCall, R., Lescinski, J., 2009. Modeling storm impacts on beaches, dunes and barrier islands. Coast. Eng. 56, 1133–1152.
Sallenger, A., 2000. Storm impact scale for barrier islands. J. Coast. Res. 16 (3), 890–895.
Scott, T., Masselink, G., Davidson, M., Russell, P., Conley, D., Siggery, E., 2015n. Impact of extreme Atlantic storms during 2013/1014 winter on the southwest coast of England (in preparation).
Smit, P., Stelling, G., Roelvink, J., Van Thiel de Vries, J., McCall, R., Van Dongeren, A., Zwinkels, C., Jacobs, R., 2010. XBeach: Non-hydrostatic model: Validation, verification and model description. Tech. rep.Delft University of Technology
Smit, P., Zijlema, M., Stelling, G., 2013. Depth-induced wave breaking in a non-hydrostatic, near-shore wave model. Coast. Eng. 76 (0), 1–16 (http://www.sciencedirect.com/science/article/pii/S0378383913000215).
Soulsby, R.L., Whitehouse, R.J.S.W., 1997. Threshold of sediment motion in coastal environments. Pacific Coasts and Ports' 97 Conference. Univ. of Canterbury, Christchurch, New Zealand.
Stéphan, P., Suanez, S., Fichaut, B., 2010. Franchissement et migration des cordons de galets par rollover. impact de la tempête du 10 mars 2008 dans l'évolution récente du sillon de talbert (côtes-d'armor, bretagne). Norois 215, 59–75.
Stéphan, P., Suanez, S., Fichaut, B., 2012. Long-term morphodynamic evolution of the sillon de talbert gravel barrier (brittany, france). Shore Beach 80 (1), 19–36.
Tolman, H.L., Chalikov, D., 1996. Source terms in a third-generation wind wave model. J. Phys. Oceanogr. 26, 2497–2518.
Tuan, T.Q., Verhagen, H.J., Visser, P., Stive, M.J.F., 2006. Numerical modelling of wave overwash on low-crested sand barriers. 30th Coastal Engineering Conference. World Scientific, San Diego.
Turner, I., Masselink, G., 1998. Swash infiltration-exfiltration and sediment transport. J. Geophys. Res. 103 (C13), 30,813–30,824.
Turner, I.L., Masselink, G., 2012. Coastal gravel barrier hydrology – observations from a prototype-scale laboratory experiment (BARDEX). Coast. Eng. 63, 13–22 (http://www.sciencedirect.com/science/article/pii/S0378383911002006).
Van der Meer, J.W., 1992. Stability of the seaward slope of berm breakwaters. Coast. Eng. 16 (2), 205–234 (http://www.sciencedirect.com/science/article/pii/037838399290037U).
Van Gent, M., 1995. Wave interaction with berm breakwaters. J. Waterw. Port Coast. Ocean Eng. 121 (5), 229–238.
Van Gent, M., 1996. Numerical modelling of wave interaction with dynamically stable structures. Proceedings of 25th Conference on Coastal Engineering, Orlando, Florida, pp. 1930–1943.
Van Hijum, E., 1976. Equilibrium profiles and longshore transport of coarse material under oblique wave attack. Proceedings of 15th Conference on Coastal Engineering, Honolulu, Hawai. vol. 1 (https://icce-ojs-tamu.tdl.org/icce/index.php/icce/article/view/3122).
Van Hijum, E., Pilarczyk, K., 1982. Equilibrium profile and longshore transport of coarse material under regular and irregular wave attack. Tech. rep.Delft Hydraulics
Van Rijn, L., 1982. Equivalent roughness of alluvial bed. J. Hydraul. Div. ASCE 108 (HY 10), 1215–1218.
Van Rijn, L., June 2007. Unified view of sediment transport by currents and waves. i: Initiation of motion, bed roughness, and bed-load transport. J. Hydraul. Eng. 133 (6), 649–667.
Van Rijn, L., Sutherland, J., 2011. Erosion of gravel beaches and barriers. Proceedings of Coastal Sediments. World Scientific Publishing Co., Inc., Miami.
Van Rijn, L., Walstra, D., Grasmeijer, B., Sutherland, J., Pan, S., Sierra, J., 2003. The predictability of cross-shore bed evolution of sandy beaches at the time scale of storms and seasons using process-based Profile models. Coast. Eng. 47 (3), 295–327 (http://www.sciencedirect.com/science/article/pii/S0378383902001205).
Van Rijn, L., Walstra, D., van Ormondt, M., 2007. Unified view of sediment transport by currents and waves. iv: Application of morphodynamic model. J. Hydraul. Eng. 133 (7), 776–793.
Williams, J., Buscombe, D., Masselink, G., Turner, I., Swinkels, C., 2012a. Barrier dynamics experiment (BARDEX): Aims, design and procedures. Coast. Eng. 63, 3–12 (http://www.sciencedirect.com/science/article/pii/S0378383911002018).
Williams, J., de Alegría-Arzaburu, A.R., McCall, R.T., van Dongeren, A., 2012 bb. Modelling gravel barrier profile response to combined waves and tides using XBeach: Laboratory and field results. Coastal Engineering. BARDEX: a large-scale laboratory study of gravel barrier dynamics 63, pp. 62–80 (http://www.sciencedirect.com/science/article/pii/S037838391100202X).
Zijlema, M., Stelling, G., Smit, P., 2011. Swash: An operational public domain code for simulating wave fields and rapidly varied flows in coastal waters. Coast. Eng. 58 (10), 992–1012 (http://www.sciencedirect.com/science/article/pii/S0378383911000974).